Absolute spectroscopic factors from the $(p,p\alpha)$ reaction at 100 MeV on $1p$-shell nuclei*

P. G. Roos, N. S. Chant, A. A. Cowley,† D. A. Goldberg, H. D. Holmgren, and R. Woody, III‡
Department of Physics and Astronomy, University of Maryland, College Park, Maryland 20742
(Received 30 August 1976)

The $(p,p\alpha)$ reaction on ^{6}Li, ^{7}Li, ^{9}Be, and ^{12}C has been investigated experimentally at a bombarding energy of 100 MeV. Data were obtained at a large number of angle pairs in order to study the reaction mechanism. The data are in good agreement with distorted-wave impulse-approximation calculations; unlike most analyses of transfer reactions we obtain absolute α-particle spectroscopic factors. These are in good agreement with $1p$ shell model predictions. Thus we find no evidence for additional α-particle-like correlations.

[NUCLEAR REACTIONS ^{6}Li, ^{7}Li, ^{9}Be, ^{12}C$(p,p\alpha)$, $E_0=100$ MeV; measured $d^3\sigma/d\Omega_p d\Omega_\alpha dE_p(\theta_p,\theta_\alpha,E_p,E_\alpha)$; coplanar geometry; DWIA analysis; deduced α-particle spectroscopic factors.]

I. INTRODUCTION

Experimental studies of cluster knockout reactions such as $(p,p\alpha)$ have been carried out for over a decade. At lower energies ($\sim$50 MeV) the reaction is often dominated by sequential processes,[1] in which the incident particle scatters inelastically from the target nucleus, leaving it in a particle unstable excited state which subsequently decays. At higher energies ($E \gtrsim 100$ MeV) the data[2-5] show evidence that the direct knockout process dominates the reaction mechanism. Thus the hope has been that the study of cluster knockout reactions at higher energies would provide quantitative information on the cluster structure of nuclei. We believe the present work marks a realization of that hope which until now has gone largely unfulfilled.

A major reason for the paucity of quantitative information extracted from cluster knockout reactions is the simplistic treatment of the reaction mechanism usually employed. In most cases knockout data have been analyzed using the plane-wave impulse approximation (PWIA). The inadequacy of this treatment has been shown many times; although attempts to improve upon it by introducing a lower radial cutoff have had limited success in a few instances,[6,7] in general this procedure is unsatisfactory.

An obvious extension of the PWIA is the distorted-wave impulse approximation (DWIA), in which the incoming and outgoing waves are distorted by suitable optical model potentials. Although DWIA calculations have been performed for $(p,2p)$ reactions,[8-12] very few[5,13-17] have been performed for cluster knockout. In the preceding paper[16] (referred to hereafter as I) a number of DWIA calculations for $(p,p\alpha)$ and $(\alpha,2\alpha)$ reactions are presented. Even for energies as high as 600 MeV, these calculations clearly show the importance of distortion effects, as well as the resultant inadequacies of PWIA treatments. Further discussions of cluster knockout reactions and their analyses using DWIA calculations are presented in Refs. 17 and 18.

In this paper we present a rather detailed experimental study of the $(p,p\alpha)$ reaction, not only as a test of the reaction mechanism, but also in an attempt to extract quantitative cluster structure information through the use of the DWIA. In particular, we have studied the $(p,p\alpha)$ reaction on ^{6}Li, ^{7}Li, ^{9}Be, and ^{12}C at a bombarding energy of 100 MeV. Data were taken for a number of angle pairs in order to test the validity of the factorized impulse approximation in a manner insensitive to the treatment of distortion effects. The accuracy of our treatment of such effects was also investigated, as was the sensitivity of the predicted absolute cross sections to the choice of distortion potentials. It is our conclusion that, at an incident energy of 100 MeV, the $(p,p\alpha)$ reaction is sufficiently well understood that it can be used to obtain reliable absolute α-particle spectroscopic factors.

II. THE EXPERIMENT

A. Experimental setup

Experimental data were obtained using a 100 MeV incident proton beam from the University of Maryland isochronous cyclotron. The experimental setup is shown schematically in Fig. 1. Since the contribution of the beam energy spread ($\sim$150 keV) to the overall energy resolution was insignificant, the beam line was operated in a so-called "nondispersive" mode in which the dispersion

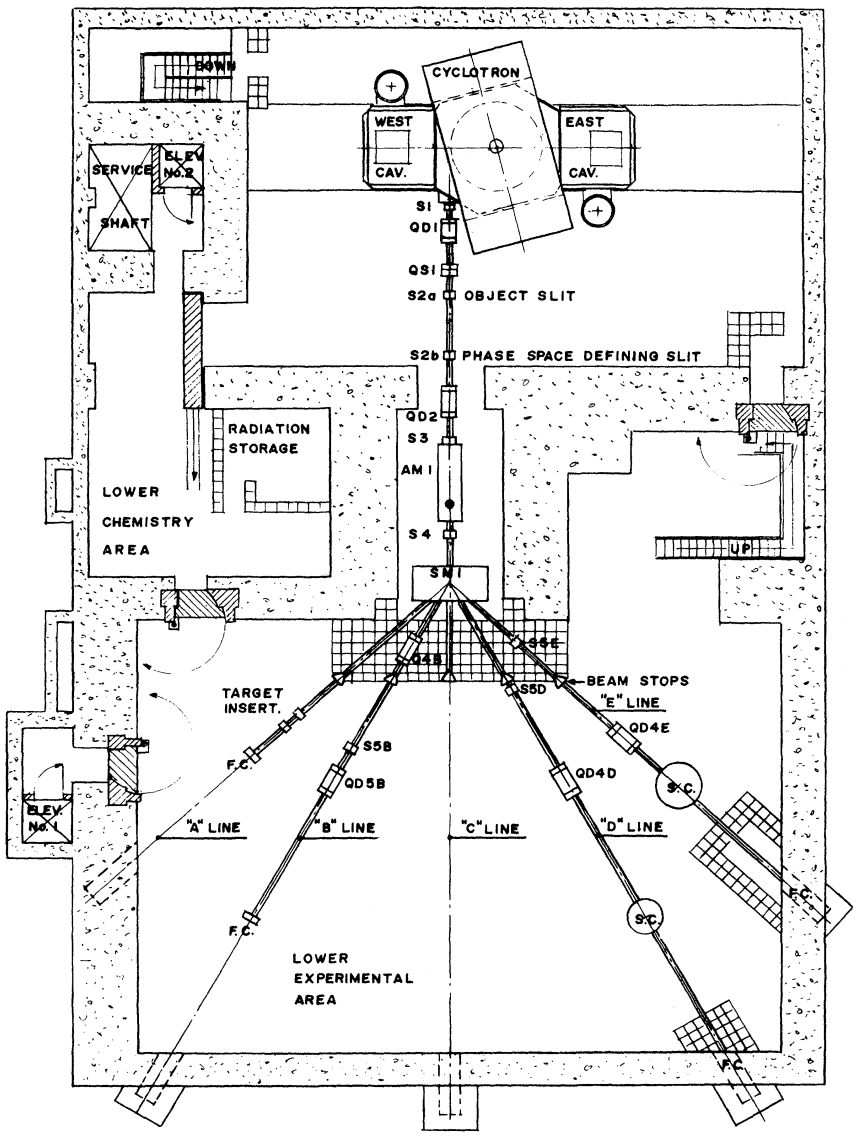

FLOOR PLAN
CYCLOTRON CAVE - LOWER EXPERIMENTAL AREA

FIG. 1. Experimental layout for the cyclotron and lower experimental area. The $(p, p\alpha)$ experiment was performed in the scattering chamber on *"E"* line.

resulting from the switching magnet SW was minimized. The beam was initially focused at S2a using quadrupole doublet QD1, and its phase space determined by slits S2a and S2b. The beam was then focused at S4 by means of the quadrupole doublet QD2. The slits at S4 were adjusted to a separation slightly greater than the size of the focused beam spot in order to reduce background, and no additional apertures were used between S4 and the target. Protons emerging from the focus at S4 were deflected through 48° by the switching magnet and brought to a final focus on a target at the center of a 150 cm diameter scattering chamber by means of a quadrupole doublet QD4. The resultant beam spot was approximately 1.5 mm wide ×3 mm high with a total angular divergence in the horizontal (scattering) plane of 8 mr. The beam was monitored by a Faraday cup behind the scattering chamber.

Targets mounted in the center of the scattering chamber were viewed by two counter telescopes mounted on arms which could be positioned remotely to ±0.02°. One counter telescope, intended primarily for proton detection, consisted of a

1 mm silicon surface barrier ΔE detector followed by a 2.5 cm diameter $\times$5 cm thich NaI(Tl) scintillation E detector. The subtended solid angle was approximately 4.83 msr. The second counter telescope, located in the scattering plane defined by the incident beam and the first counter telescope, was intended primarily for α-particle detection and was located on the opposite side of the incident beam. It consisted of a 200 μm silicon surface barrier ΔE detector followed by a 3 mm lithium-drifted silicon detector and subtended 1.21 msr. Signals from all four detectors were fed to preamplifiers mounted inside the scattering chamber. For the scintillation counter a conventional emitter follower circuit was used, while charge sensitive preamplifiers[19] were used for the three silicon detectors. For the two ΔE detectors additional fast outputs from time pickoff units in the preamplifiers were amplified, fed to constant fraction discriminators,[20] and used to start and stop a time-to-amplitude converter (TAC). This recorded the relative time of events in the two detector systems to within 1.5 ns. The four ΔE and E linear signals were amplified and a fivefold slow ($\sim$1 μs) coincidence between these signals and the TAC linear output signal was used to provide an overall gating signal for the entire system. After passing through linear gates the five signals were digitized using 100 MHz analog to digital converters which were interfaced to an IBM 360/44 computer. Since the TAC range encompassed several beam pulses ($\sim$60 ns apart), both real and random coincidences were recorded simultaneously. In addition, a pulser system, connected to the four detector preamplifiers and triggered at a rate proportional to the incident beam intensity, simulated coincident events thus permitting an estimate of counting losses due to electronic deadtime.

Data handling was achieved with a computer code P2P which permitted great flexibility.[21] In the code, energy calibrations, energy additions, and particle identification were performed for each event. Five one-dimensional arrays (one 512 channel, two 1024 channels, two 2048 channels) were available for the display of various unconverted or calculated quantities. In addition, a two-dimensional 128$\times$128 channel array was available to display correlated quantities. Typical one-dimensional displays used during data acquisition included the entire summed energy spectrum of telescope 1 ($E_p = E1 + \Delta 1$) or telescope 2 ($E_\alpha = E2 + \Delta 2$), the TAC spectrum, the particle identification spectra for the two telescopes, and the binding energy spectrum [$F3 = E_p + E_\alpha + E_B = E_0 + Q$, where we are considering a reaction $A(p,p\alpha)B$ and E_B is the calculated recoil energy of the undetected residual nucleus]. The two-dimensional array was used initially to set up the particle identification for both telescopes. Once the experiment was in progress a two-dimensional display of E_p vs E_α or $F3$ vs E_p was usually selected. All analyzers could be gated by software windows set on any of the calibrated or calculated quantities. For example, the two-dimensional display of E_p vs E_α was generally gated by windows on the particle identification spectra (p and α) and the real coincidence peak in the TAC spectrum. In addition, all raw data events were written on magnetic tape to permit subsequent detailed analysis, including other reaction channels such as $(p, d^3\mathrm{He})$.

Due primarily to the energy resolution of the NaI crystal, the best energy resolution obtained in the binding energy spectra was approximately 1 MeV full width at half maximum (FWHM). In addition, small nonlinearities in the proton telescope led to approximately a 1% uncertainty in the proton energy determination. The uncertainty in the determination of the recoil momentum of the residual undetected nucleus (i.e., the recoil momentum resolution) due to the finite solid angles and finite energy resolution was calculated using the code MOMRATH.[7] Typical results indicate a momentum resolution of approximately 13 MeV/c (FWHM) for small recoil momenta.

The data were taken in three separate runs, each with the identical experimental setup. The target thicknesses are listed in Table I. Also listed in Table I are the errors in absolute cross section associated with the data for each target, the differences primarily reflecting the accuracy in the determination of target thickness. The errors presented in the subsequent figures are statistical errors only.

B. Experimental data

Angle pairs $(\theta_p, \theta_\alpha)$ were generally chosen so that the residual undetected nucleus was left with small recoil momentum $\vec{p}_B$. Primary emphasis was placed on quasifree angle pairs, i.e., those angle pairs for which it is kinematically allowed

TABLE I. Target and absolute cross section information.

Target	Thickness (mg/cm^2)	Isotopic purity	Absolute error in $d^3\sigma/d\Omega_p d\Omega_\alpha dE_p$
		(%)	(%)
^{6}Li	0.22 4.90	99	15
^{7}Li	10.2	99	20
^{9}Be	2.42	100	15
^{12}C	2.27	Polystyrene (91 ^{12}C)	15

for the residual nucleus to be left at rest. Typical binding energy spectra (excitation energy spectra of the residual nucleus) for each target are presented in Fig. 2. With the exception of the $^{12}C(p,p\alpha)^{8}Be$ reaction no excited states of the residual nucleus are observed. In the case of ^{8}Be we observe the first excited state (2+), and some slight indication of a state near 16 MeV excitation.

For each state in the residual nucleus the correlation data for a given angle pair were projected onto the proton energy axis forming the energy sharing triple differential cross section $d^3\sigma/d\Omega_p d\Omega_\alpha dE_p$. Typical energy sharing cross sections for one of the quasifree angle pairs are presented in Fig. 8 in Sec. IV. The point corresponding to zero recoil momentum of the residual nucleus is indicated by an arrow on the proton energy axis. A tabulation of all angle pairs studied for each target is presented in Table II along with the minimum recoil momentum and the three-body cross section at that point.

Several observations can be made. Firstly, the data for each state for which the knockout of an α particle carrying angular momentum $L=0$ is al-

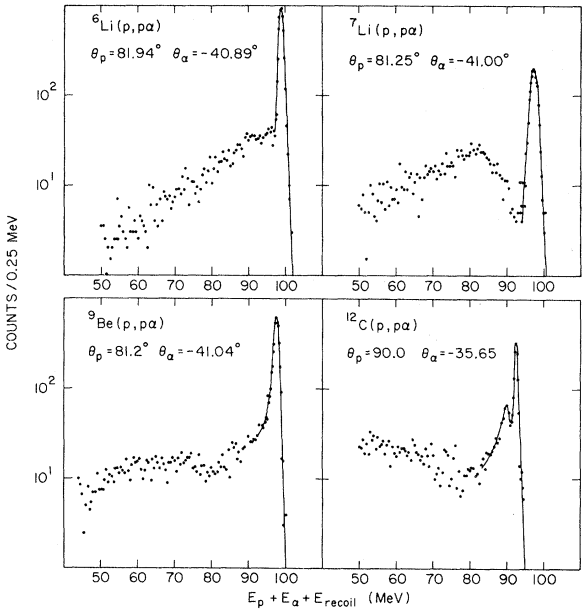

FIG. 2. Binding energy spectra ($F3 = E_p + E_\alpha + E_B$) for the $(p,p\alpha)$ reaction on the various targets. Due primarily to the thickness of the ΔE detectors these spectra represent events with $E_p \geq 14$ MeV and $E_\alpha \geq 18$ MeV.

TABLE II. Angle pairs and cross sections at minimum recoil momentum for each target.

Reaction	θ_p/θ_α (deg)	$P_{B,\mathrm{Min}}$ (MeV/c)	$d^3\sigma/d\Omega_p d\Omega_\alpha dE_p$ $\frac{\mathrm{mb}}{\mathrm{sr^2\,MeV}}$
$^{6}Li(p,p\alpha)^{2}H$	45.0/−71.5	63	$(2.00\pm0.18)\times10^{-1}$
	60.0/−52.7	0	(1.07 ± 0.05)
	60.0/−57.4	34	$(4.40\pm0.22)\times10^{-1}$
	75.0/−44.5	0	$(4.07\pm0.20)\times10^{-1}$
	75.0/−45.7	11	$(3.77\pm0.19)\times10^{-1}$
	81.9/−40.9	0	$(2.35\pm0.12)\times10^{-1}$
	90.0/−35.8	11	$(9.84\pm1.08)\times10^{-2}$
	90.0/−36.8	0	$(1.03\pm0.07)\times10^{-1}$
	105.0/−27.5	23	$(2.16\pm0.50)\times10^{-2}$
	105.0/−29.7	0	$(3.77\pm0.41)\times10^{-2}$
$^{7}Li(p,p\alpha)^{3}H$	75.0/−45.3	0	$(1.03\pm0.08)\times10^{-2}$
	81.3/−41.0	0	$(7.98\pm0.64)\times10^{-3}$
	105.0/−29.5	0	$(1.90\pm0.38)\times10^{-3}$
$^{9}Be(p,p\alpha)^{5}He$	60.0/−52.4	0	$(1.94\pm0.10)\times10^{-1}$
	60.0/−60.3	56	$(7.11\pm0.57)\times10^{-2}$
	75.0/−44.3	0	$(6.98\pm0.35)\times10^{-2}$
	75.0/−49.0	40	$(5.41\pm0.27)\times10^{-2}$
	75.0/−56.8	10	$(1.51\pm0.09)\times10^{-2}$
	81.2/−41.0	0	$(4.48\pm0.22)\times10^{-2}$
	90.0/−36.6	0	$(3.20\pm0.22)\times10^{-2}$
	105.0/−30.9	14	$(1.86\pm0.20)\times10^{-3}$
$^{12}C(p,p\alpha)^{8}Be(0+)$	75.0/−43.1	0	$(8.99\pm1.17)\times10^{-3}$
	90.0/−35.7	0	$(4.87\pm0.63)\times10^{-3}$
	105.0/−28.7	0	$(1.86\pm0.24)\times10^{-3}$
$^{12}C(p,p\alpha)^{8}Be(2+)$	75.0/−43.1	2	$(9.61\pm0.96)\times10^{-3}$
	90.0/−35.7	2	$(2.55\pm0.41)\times10^{-3}$
	105.0/−28.7	2	$(9.87\pm1.88)\times10^{-4}$

lowed show a broad peak centered at a recoil momentum $\vec{p}_B \simeq 0$ MeV/c. The data for the reaction ^{7}Li$(p,p\alpha)^3$H which must proceed by the knockout of an $L=1$ α particle show a pronounced minimum near zero recoil momentum. These results support the knockout interpretation of the data. Somewhat surprisingly, the ^{8}Be(2+) state does not show the expected minimum for $L=2$ α cluster knockout. However, since this state is unbound, the possibility of a mixed angular momentum transition exists which could allow an $L=0$ component to fill in the minimum[22]; this point is discussed in Sec. IV. Secondly, we see that each data set includes narrow sequential peaks corresponding to the process $[p+A \rightarrow p+A^* \rightarrow (A-4)+\alpha]$ at the upper end of the proton energy spectrum. For ^{12}C$(p,p\alpha)^8$Be these states extend up to ~30–35 MeV excitation energy in ^{12}C, and do cause some interference with the quasifree peak. Finally, the cross section decreases by approximately a factor of 20 from ^{6}Li to ^{12}C.

III. DWIA CALCULATIONS

The theoretical analysis of the data was performed using the DWIA. Following the derivation in I, the triple differential cross section for the $A(p,p\alpha)B$ reaction can be written in the form

$$\frac{d^3\sigma}{d\Omega_p\, d\Omega_\alpha\, dE_p} = \mathrm{KF}\,\{S_\alpha |\, \phi(-\vec{p}_B)\,|^2\}\, \frac{d\sigma}{d\Omega}\bigg|_{p-\alpha}, \quad (1)$$

where KF is a kinematic factor. Comparing Eq. (1) with Eq. (17) of I, we see that $|\langle \bar{t} \rangle|^2$ has been reexpressed in terms of $d\sigma/d\Omega\,|_{p-\alpha}$, the corresponding unpolarized cross section. In addition, since for $(p,p\alpha)$ reactions $C^2=1$ and $L=J$, it is convenient to replace the product $C^2 S_{LJ}$ appearing in I by S_α. Finally,

$$|\, \phi(-\vec{p}_B)\,|^2 = \sum_\Lambda |\, T_{BA}^{\alpha L\Lambda}\,|^2 \quad (2)$$

we shall refer to as the "distorted momentum distribution."

In the DWIA the two-body cross section $d\sigma/d\Omega\,|_{p-\alpha}$ is properly a half-off-the-energy shell cross section. Typically, some prescription is chosen to replace $d\sigma/d\Omega\,|_{p-\alpha}$ by a nearby measured on-shell cross section. This leads to an ambiguity in $d\sigma/d\Omega\,|_{p-\alpha}$. In order to investigate the importance of off-energy shell effects, we have calculated the half-shell p-α cross sections for various α-particle binding energies using optical model potentials from an analysis of 85 MeV p-α elastic scattering.[23] The calculations use the full potential including the Majorana exchange term, but excluding Coulomb effects. The effect of the Coulomb potential was shown to be unimportant except at the smallest angles ($\theta \leq 10°$) by calculating the on-shell cross section with and without the Coulomb term. The half-shell calculations are similar to those presented in Refs. 7 and 18. Calculations were performed for values of Δ, the distance off shell, ranging from 0 to −20 MeV, using both the final energy method (plane-wave initial state and full-scattered-wave final state) and the initial energy method (full-scattered-wave initial state and plane-wave final state) which are identified by T^{I} and T^{II}, respectively, in Ref. 7.

In Fig. 3(a) we present results for the final energy method utilizing the potential $V1$ (volume imaginary potential) of Ref. 23. With the exception of the region near the minimum, the off-shell effects are quite small, particularly when one considers that, in the region of interest ($\vec{p}_B \simeq 0$) for the target nuclei studied here, $\Delta \leq -10$ MeV. Calculations using the initial energy method show similar effects; i.e., the only significant differences occur in the region of the minimum. A second p-α potential with a surface imaginary potential (potential $S1$ of Ref. 23) gives rise to effects even smaller than those shown in Fig. 3(a).

In Fig. 3(b) we show a comparison between the half-shell cross sections for $\Delta = -10$ and −20 MeV and the on-shell cross sections at the final energy obtained with the same optical potential. The on-shell cross sections have been multiplied by the ratio of the final and initial momenta of the proton in order to remove the two-body phase space differences between the two cross sections. The differences between the two curves are again quite small, particularly for $\Delta = -10$ MeV. This comparison suggests that the use of the two-body on-shell cross section corresponding to the final two-body energy is adequate in the present analysis.

Based on the above comparisons, the fact that off-shell effects are small, experimental results which suggest that the final energy is the appropriate two-body energy,[7,24,25] and, finally, the fact that the final energy method arises as the first term of a multiple scattering expansion based on the Faddeev equations,[26] we have chosen to use the on-shell p-α cross sections corresponding to the final state (energy and angle) of the two-body system. This is generally referred to as the final energy prescription. Where necessary, the p-α cross sections were obtained from a polynominal interpolation of available elastic scattering data.[27]

Following Eq. (30) of I the amplitude $T_{BA}^{\alpha L\Lambda}$ may be written

$$T_{BA}^{\alpha L\Lambda} = \frac{1}{(2L+1)^{1/2}} \int \chi_p^{(-)*}(\vec{\mathbf{r}})\, \chi_\alpha^{(-)*}(\vec{\mathbf{r}})\, \chi_{p_0}^{(+)}(\gamma\vec{\mathbf{r}}) \times \phi_{L\Lambda}^{\alpha}(\vec{\mathbf{r}})\, d\vec{\mathbf{r}}\,, \quad (3)$$

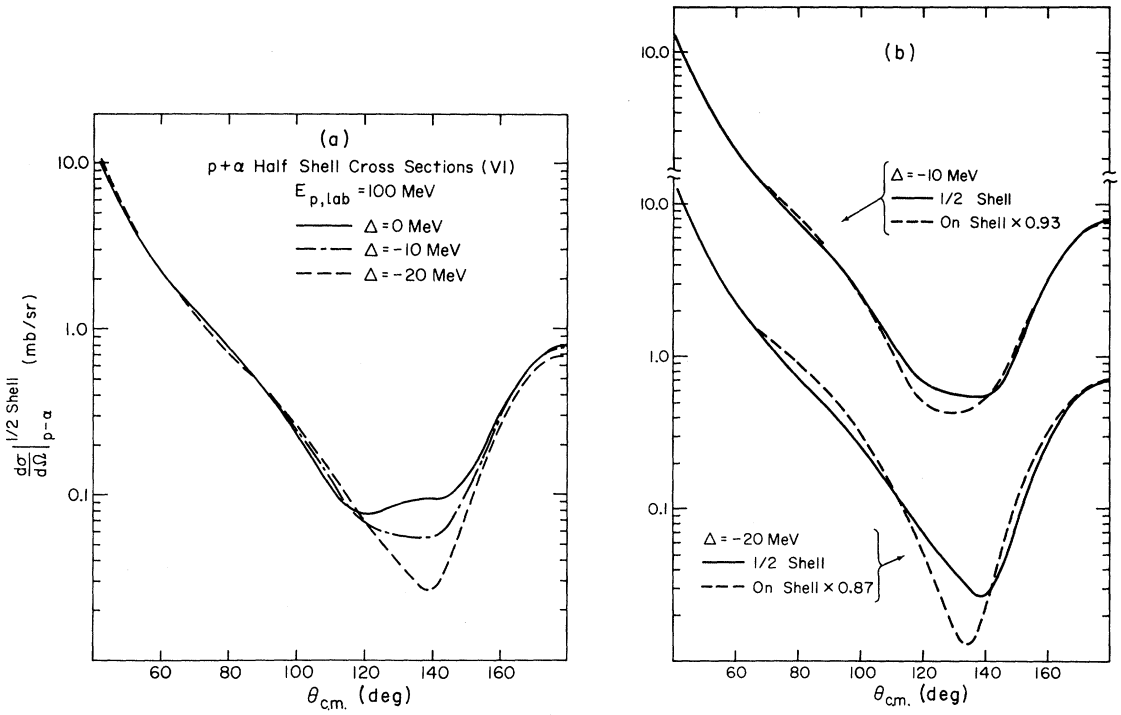

FIG. 3. (a) The half-shell p-α cross sections obtained using the final energy procedure and the potential $V1$ of Ref. 23. The calculations are off shell by the quantity Δ specified on the figure. (b) Comparison of the half-shell cross section and the on-shell cross section at the final energy multiplied by the ratio of the final to initial center-of-mass momentum. The calculations are off shell by 10 and 20 MeV. The calculations utilize potential $V1$ of Ref. 23.

where $\gamma = B/A$, the χ's represent incoming and outgoing distorted waves, and $\phi^{\alpha}_{L\Lambda}(\vec{r})$ is the wave function of the α cluster in the target nucleus. It is easy to show that in the PWIA this expression is simply the Fourier transform of the α-cluster wave function at an α-particle momentum $-\vec{p}_B$. Thus, in the plane-wave limit $|\phi(-\vec{p}_B)|^2$ reduces to the momentum distribution of the struck α cluster. As discussed in I, we can expect this result to be modified significantly by distortion effects which typically reduce the contributions of the nuclear interior to $\phi(-\vec{p}_B)$. Thus in practice the knockout reaction is strongly localized in the surface region.

The bound α-cluster wave function $\phi^{\alpha}_{L\Lambda}(\vec{r})$ strictly represents the result of projecting the target nucleus wave function onto the product of the residual nucleus wave function and the internal wave function of an α particle in its ground state. Following common practice in both knockout and transfer reaction analysis we have replaced this quantity by an eigenfunction of a Woods-Saxon potential with an energy eigenvalue corresponding to the α-particle separation energy. The principle quantum number of this wave function is chosen on the basis of conservation of oscillator-shell-model quanta. Only that portion of the oscillator wave function involving zero quanta for relative motion of the four nucleons is retained and all oscillator quanta are associated with the center-of-mass motion of the α cluster; thus, assuming $(1s^4)(1p^n)$ configurations, for ^{12}C and ^{9}Be the α cluster is assumed to be in a $3S$ or $2D$ state, while for ^{7}Li and ^{6}Li the quantum numbers are $2P$ and $2S$, respectively.

The geometry of the Woods-Saxon well for the bound α particle was obtained with a folding model technique. The folding model has had reasonable success in providing real optical potentials for low energy elastic α scattering[28,29] and recently has provided bound state properties for nuclei in the s-d shell.[30] Although there are difficulties with the folding model, it at least provides a reasonable approach for obtaining an α-bound state potential and, more importantly, determines the variation in the well geometry with target nucleus. This variation is important for such light systems as the p-shell nuclei.

Our particular approach was to fold the α-nucleon interaction from Ref. 29 into charge distributions obtained from electron scattering for a series of nuclei between $A=6$ and $A=40$. The resultant potential was then replaced by a Woods-Saxon potential which had the same half radius

and rms radius. This procedure determined the radius r_0 and diffuseness a of the Woods-Saxon well as a function of A. The required values for the nuclei studied here were then obtained by interpolation. The resultant geometrical parameters are presented in Table III. For each target nucleus the well depth was adjusted to reproduce the empirical α-particle separation energy. The sensitivity of the DWIA calculations to variations in the bound state geometry is presented in Sec. IV. It will be seen that the effects are not particularly large, and that the primary effect is on the magnitude of the cross section due to the surface localization.

Optical potentials used in the calculations of the incoming and outgoing distorted wave channels were taken from various sources.[15,31-34] Particular difficulty was found in obtaining suitable α-particle optical potentials for these light systems. The optical model potentials used in the calculations, along with their sources, are listed in Table III. Since the DWIA code is restricted to central optical potentials, the spin-orbit parts of the proton potentials have been omitted. Some variation of the optical potentials was carried out in order to investigate the sensitivity of the calculations to the optical potentials. These are also discussed in Sec. IV.

IV. ANALYSIS OF DATA

The analysis of the experimental data was separated into three parts. Firstly, we considered experimental tests of the reaction mechanism which are largely independent of the distortion effects, at least in the DWIA. (The neglect of distortion in these comparisons was justified by numerical calculations.) Secondly, the DWIA calculations were compared directly to the experimental data to investigate both the quality of the fits to the data in terms of shape, and to extract the α-particle spectroscopic factors S_α. Finally, we investigated the effects on the spectroscopic factors of variations of the bound state and optical model parameters used in the DWIA calculations.

A. Tests of the reaction mechanism

In an attempt to isolate effects due to the factorization approximation we have divided the experimental differential cross sections by the kinematic factor KF. In DWIA we have

TABLE III. Optical potential parameters. The optical potential is defined to be

$$V_{\rm opt} = -Vf(r,r_0,a) - i\left(W - 4W_D a' \frac{d}{dr'}\right) f(r,r'_0,a') + V_{\rm Coulomb},$$

where

$$f(r,r_0,a) = [1 - \exp\left(\frac{r - r_0 A^{1/3}}{a}\right)]^{-1};$$

A is the target mass; $V_{\rm Coulomb}$ is the Coulomb potential of a uniform sphere of charge of radius $r_c A^{1/3}$.

Reaction	System	V	r_0	a	r_c	W	W_d	r'_0	a'	Ref.
^{6}Li$(p,p\alpha)^2$H	$p+^6$Li [a]	16.6	1.16	0.75	1.80	0.1	3.9	1.37	0.63	15,31
	$p+^2$H	4.5	1.60	0.50	1.60	8.4	0	1.60	0.50	15
	$\alpha+^2$H	91.8	1.32	0.70	1.30	0	8.3	1.39	0.75	15
	Bound state	77.0	1.47	0.71	1.47					15
^{7}Li$(p,p\alpha)^3$H	$p+^7$Li [a]	17.5	1.33	0.65	1.83	11.6	0	1.46	0.44	31
	$p+^3$H	15.4	1.42	0.15	1.30	0	10.1	1.51	0.31	23
	$\alpha+^3$H	158.0	0.70	0.86	1.41	14.7	0	2.10	0.48	34
	Bound state	91.9	1.43	0.72	1.43					
^{9}Be$(p,p\alpha)^5$He	$p+^9$Be [a]	19.3	1.33	0.65	1.89	10.5	0	1.46	0.44	31
	$p+^5$He	37.8	1.14	0.79	1.30	0	4.5	1.32	0.48	32
	$\alpha+^5$He	88.9	0.99	0.81	1.20	4.9	0	3.01	0.58	33
	Bound state	89.3	1.35	0.73	1.35					
^{12}C$(p,p\alpha)^8$Be	$p+^{12}$C [a]	21.2	1.33	0.65	1.33	6.5	0	1.46	0.44	31
	$p+^8$Be	32.3	1.26	0.63	1.30	0	2.3	1.31	0.96	32
	$\alpha+^8$Be	88.9	0.99	0.81	1.20	4.9	0	3.01	0.58	33
	Bound state	89.9	1.23	0.75	1.23					

[a] These well depths were multiplied by B/A in order to exclude crudely the interaction of the incoming proton with the knocked out α particle.

$$\frac{d^3\sigma}{d\Omega_p\, d\Omega_\alpha\, dE_p}/\mathrm{KF} = \{S_\alpha |\, \phi(-\vec{p}_B)|^2\}\frac{d\sigma}{d\Omega}\bigg|_{p-\alpha}. \quad (4)$$

In principle S_α is a constant. In addition, explicit DWIA calculations of $|\,\phi(-\vec{p}_B)|^2$ for ^{6}Li, ^{9}Be, and ^{12}C at $\vec{p}_B = 0$ MeV/c show that this quantity varies by less than 10% over the entire angular range of the experimental data. Thus, in the factorized DWIA, the ratio constructed in Eq. (4) should be proportional to the two-body cross section $d\sigma/d\Omega|_{p-\alpha}$ to better than 10%. For the three $L=0$ transitions studied we have plotted the ratio $(d^3\sigma/d\Omega_p\, d\Omega_\alpha\, dE_p)/\mathrm{KF}$ for $\vec{p}_B = 0$ MeV/c for each quasifree angle pair as a function of the p-α center-of-mass scattering angle calculated for the final state. (Similar tests of the factorization approximation can be found in Refs. 7, 15, 24, and 35.) These results, each set normalized to the free p-α cross section at 100 MeV (Ref. 36) at approximately 90°, are presented in Fig. 4. Although the data is somewhat sparse we see an interesting trend. While the ^{6}Li data agree very well with the free cross section data, the ^{9}Be and ^{12}C data show a decreased slope compared to the free cross section data, the effect being more pronounced for ^{12}C. Since the α cluster binding energy (BE) increases smoothly from ^{6}Li (BE = 1.47 MeV) to ^{12}C (BE = 7.37 MeV), one might speculate that this breakdown in the factorization approximation is a manifestation of off-energy shell effects. Since the calculations presented in Sec. III show no strong off-shell effects, this is unlikely, although other p-α potentials might exhibit somewhat different off-shell behavior.

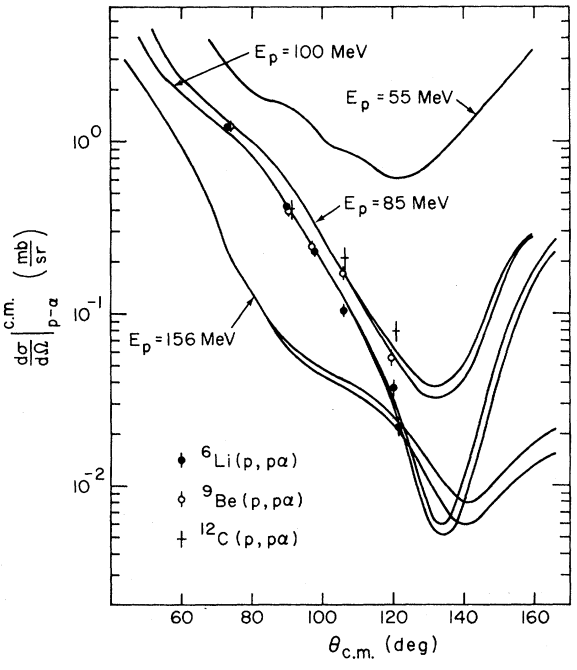

FIG. 4. Quasifree angular distributions for the $L=0$ $(p,p\alpha)$ transitions. The curves are free p-α cross sections at various energies, the double lines reflecting the relative errors. The $(p,p\alpha)$ results have been normalized near 90°.

In an attempt to understand this breakdown in factorization, we have performed DWIA calculations to investigate the region of sensitivity for each target nucleus. Histograms[16] of the radial contributions $\Delta\sigma$ to the DWIA cross sections for the transitions shown in Fig. 4 are plotted as a function of radius for each target nucleus in Fig. 5. As discussed in I, strong surface localization is characteristic of these reactions, indicating little sensitivity to details of the nuclear interior. However, it is significant that in the transition from ^{6}Li to ^{12}C the region in which the contributions to the calculated cross section are significant moves to smaller radii. For example, the arrow specifying the radius for which one-half the contribution lies outside of that radius moves in by more than 1 fm. Thus, for ^{6}Li a large part of the contributions to the DWIA cross section lie well outside the range of the nuclear potentials, where the distorted waves have their asymptotic momenta. In contrast, for ^{12}C, since the nuclear potential radius is increasing by roughly $A^{1/3}$, a significant contribution to the cross section arises within the range of the nuclear potentials. In this case the p-α interaction is often taking place inside the nuclear well and the p-α cross section may be affected. Crudely we would argue that since the nuclear potentials are attractive the p-α interaction takes place at a higher energy. Examination of the p-α data in Fig. 4 shows that at higher energies ($E_p = 156$ MeV) the p-α cross section is flattening off in the angular region of the experiment. Thus, the preceding arguments suggest that the breakdown in factorization is consistent with the fact that the p-α interaction is taking place within the nuclear well. Improved calculations such as a full finite range distorted-wave calculation employing a pseudopotential or an expansion procedure such as that suggested by Redish[37] are not at present available. Thus, although some breakdown in factorization is evident, the resultant α-particle spectroscopic factors even for ^{12}C are expected to be good to a factor of 2.

A second test of the reaction mechanism, again assuming distortion effects to be relatively constant with angle, is a comparison of the shapes of the experimental spectra for different angle pairs.

Rewriting Eq. (4) as

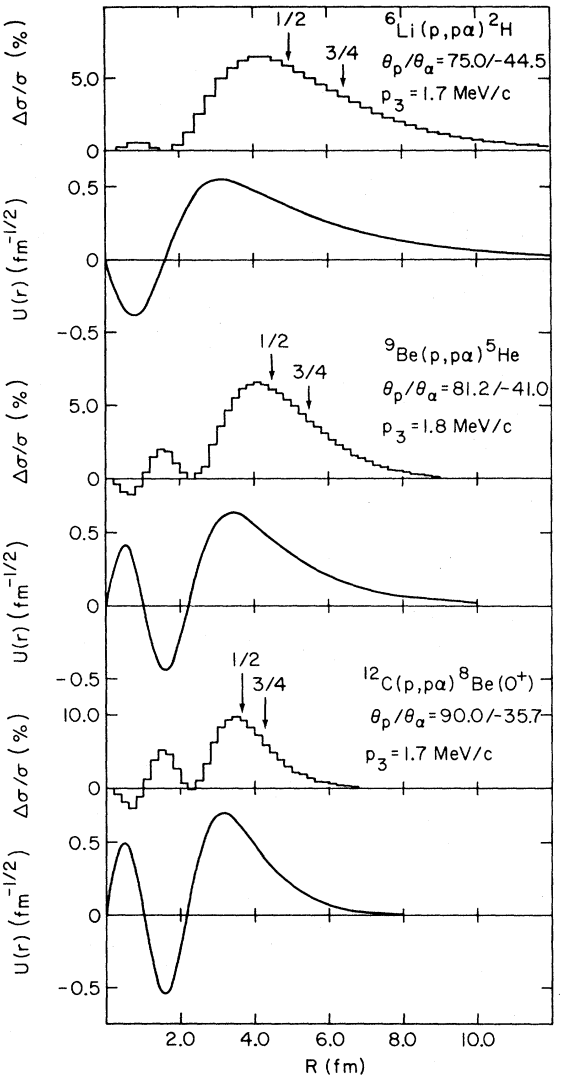

FIG. 5. Histograms of the contribution $\Delta\sigma$ to the DWIA cross section close to zero recoil momentum as a function of radius for the $L=0$ transitions. Also shown are the α-particle wave functions calculated using the Woods-Saxon wells of Table III. The arrow labeled $\frac{1}{2}$ ($\frac{3}{4}$) indicates the radius at which the cross section has risen to $\frac{1}{2}$ ($\frac{3}{4}$) of its full value.

$$\frac{d^3\sigma}{d\Omega_p d\Omega_\alpha dE_p} \Big/ \left\{ \mathrm{KF} \left. \frac{d\sigma}{d\Omega} \right|_{p-\alpha} \right\} = \{ S_\alpha | \, \phi(-\vec{p}_B) \, |^2 \}, \tag{5}$$

we obtain the distorted momentum distribution, which may be plotted versus the magnitude of the recoil momentum $\vec{p}_B$. In the PWIA this quantity simply represents the Fourier transform of the α-cluster wave function, and is therefore independent of angle. In the DWIA explicit calculations show only small changes in shape for the angle pairs studied in the present experiment. Thus instead of a comparison between the experimental data and DWIA calculations for each angle pair, a more efficient procedure is to compare the shapes of the spectra [Eq. (5)] for different angle pairs, and to carry out detailed DWIA calculations for only a small subset of these data.

The comparison of shapes was separated into two parts. First the data $(d^3\sigma/d\Omega_p d\Omega_\alpha dE_p)/\{\mathrm{KF}\, d\sigma/d\Omega|_{p-\alpha}\}$ were compared for quasifree angle pairs by normalizing different angle pairs near $\vec{p}_B = 0$. Ignoring the sequential contributions, the agreement in shape between various angle pairs is excellent. Typical results for ^{7}Li and ^{9}Be are presented in Fig. 6. Within the experimental errors we find the shapes to be constant and therefore in excellent agreement with the DWIA predictions. Thus our procedure was to perform detailed DWIA calculation for one angle pair, and additional calculations primarily for points near zero recoil momentum at other angles for normalization purposes.

A second shape comparison was made for ^{9}Be

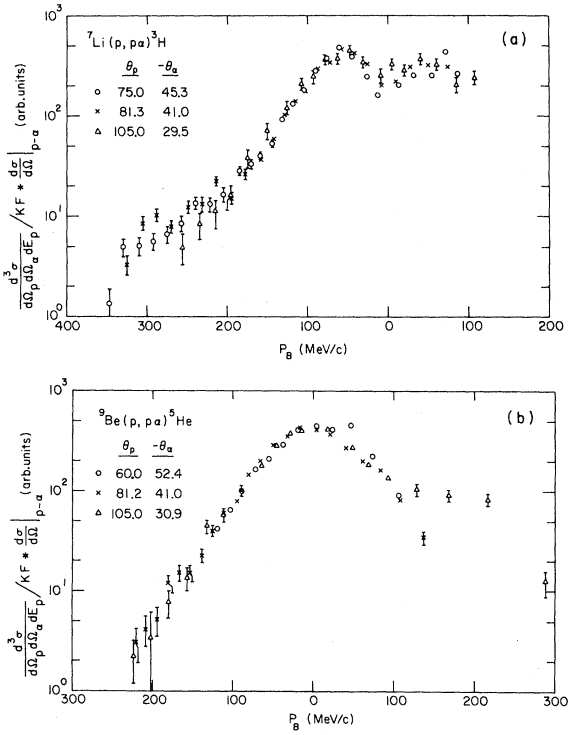

FIG. 6. (a) Plot of $(d^3\sigma/d\Omega_p d\Omega_\alpha dE_p)/\mathrm{KF}d\sigma/d\Omega|_{p-\alpha}$ versus recoil momentum for ^{7}Li at several quasifree angle pairs. The right-hand sides of the spectra show sequential contributions. (b) Plot of $(d^3\sigma/d\Omega_p d\Omega_\alpha dE_p)/\mathrm{KF}d\sigma/d\Omega|_{p-\alpha}$ versus recoil momentum for ^{9}Be at several quasifree angle pairs. The right-hand sides of the spectra show sequential contributions.

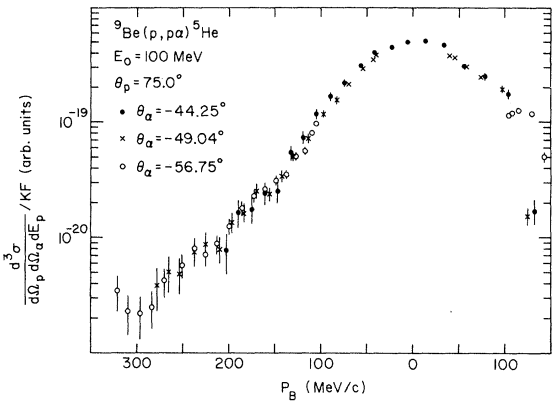

FIG. 7. Plot of $(d^3\sigma/d\Omega_p d\Omega_\alpha dE_p)/\mathrm{KF}$ versus recoil momentum for ^{9}Be with θ_p fixed and three separate α-particle angles. The right-hand sides of the spectra show sequential contributions.

for which data were available at a fixed proton angle and several α-particle angles. In this case the two-body cross section $d\sigma/d\Omega|_{p-\alpha}$ for a given E_p is nearly constant–independent of the α-particle angle. Thus in this comparison we have not bothered to remove the two-body cross section. These results are presented in Fig. 7. Again we see excellent agreement between the various data sets, in agreement with direct knockout DWIA considerations.

B. Comparison of DWIA calculations with experimental data

In the previous section we showed that the data were reasonably consistent with a DWIA interpretation of the reaction mechanism. There is some difficulty with the factorization approximation, particularly for ^{12}C, but this is not large enough to invalidate the basic interpretation in terms of the DWIA. We now present direct comparisons of the DWIA calculations to the experimental data.

Figures 8(a)–8(e) show the comparison between the DWIA calculations and the energy sharing data for one particular quasifree angle pair. The DWIA calculations have been normalized to the experimental data. These calculations utilize the potentials listed in Table III which were chosen to be most appropriate for $\vec{p}_B \simeq 0$. No corrections were made for the energy dependence of the optical potentials. A few sample calculations were performed including the energy dependence of the optical model potentials, and the effects were found to be realtively small. Thus, considering that due to the strong surface localization the basic information contained in these knockout data lies in the normalization at low recoil momentum, we have performed most calculations with the energy independent potentials of Table III.

For completeness we have also shown many of the PWIA calculations normalized to the experimental data. One observes that the PWIA calculations are completely inadequate, as discussed in I. The PWIA calculations are significantly larger than the DWIA calculations, thus showing the strong effect of absorption. The ratio of the DWIA to PWIA is indicated in Fig. 8, and shows that distortion effects decrease the cross section (at p_B near 0) by a factor of ~2 to ~10 over this range of nuclei. An equally glaring discrepancy occurs in the shapes, namely that deep minima predicted by the PWIA calculations do not occur in the experimental data; introducing a radial cutoff will not remove these minima. In contrast, the momentum smearing of the incoming and outgoing waves in the DWIA calculations removes the minima and one obtains good agreement with the experimental data.

For ^{6}Li$(p,p\alpha)^2$H [Fig. 8(a)] the agreement in shape is good except at low proton energies and has been discussed in detail in Ref. 15. For ^{7}Li$(p,p\alpha)^3$H [Fig. 8(b)] the observed disagreement in the minimum is largely removed by finite-solid-angle and energy-resolution considerations. There is also some tendency for the DWIA calculations to be slightly too broad, a problem which may be due to either the bound state wave function or the optical potentials.

In the case of ^{9}Be$(p,p\alpha)^5$He both target and residual nuclei have $J^\pi = \frac{3}{2}^-$ so that both $3S$ and $2D$ α cluster knockout is possible. In $1p$ shell model calculations[38] Kurath finds these possibilities to be equally probable. In Fig. 8(c) an equal admixture of $L=0$ and $L=2$ terms is seen to improve agreement with experiment although the $L=2$ admixture has little effect near the peak at $p_B = 0$ MeV/c and the precise relative admixture cannot be well determined from experiment. Finally, in the case of ^{12}C$(p,p\alpha)^8$Be we find quite good agreement for the ground state transition [Fig. 8(d)]. However, for the 2.90 MeV first excited state of ^{8}Be the $L=2$ calculation bears little resemblance to the data [Fig. 8(e)]. In fact, the data more nearly resemble the $L=0$ ground state transition. This observation suggests that the 2+ results may be a manifestation of the unbound nature of this state, allowing $L=0$ knockout leading to a relative $L=0$ α-α scattering state. Similar effects are observed in the ^{6}Li$(p,2p)^5$He reaction.[22] In an attempt to understand this phenomenon we have used the Watson-Migdal final state interaction technique discussed in Ref. 22. In particular, the ^{12}C$(p,p\alpha)^8$Be $L=0$ yield as a function of the ^{8}Be excitation energy E is given by

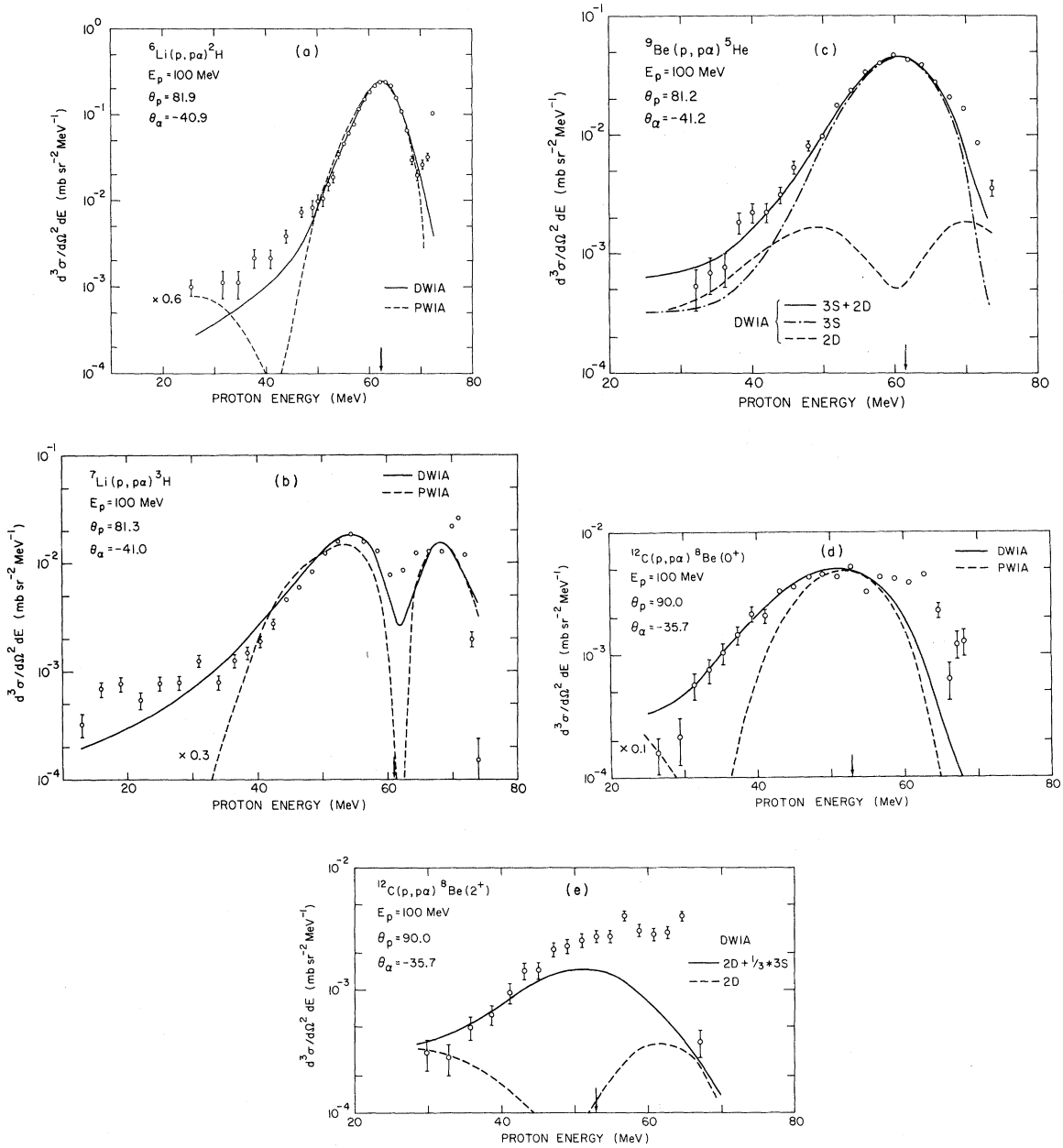

FIG. 8. (a) ^{6}Li$(p,p\alpha)$ ^{2}H energy sharing, triple differential cross section versus E_p for a quasifree angle pair. The full (dashed) curve is a DWIA (PWIA) calculation normalized to the data. The ratio of DWIA to PWIA is 0.6. (See text for details.) (b) ^{7}Li$(p,p\alpha)$ ^{3}H cross section. The ratio of DWIA to PWIA is 0.3. (c) ^{9}Be$(p,p\alpha)$ ^{5}He cross section. The curves are DWIA calculations for $L=0$ and $L=2$ knockout with equal spectroscopic strengths. (d) ^{12}C$(p,p\alpha)$ ^{8}Be(0+) cross section. The ratio of DWIA to PWIA is 0.1. (e) ^{12}C$(p,p\alpha)$ ^{8}Be(2.9 MeV) cross section. The curves are DWIA calculations for $L=0$ and $L=2$ knockout. (See text for details.)

$$Y(E) = A \sin\beta(E)/P(E),$$

where A is the normalization, β is the S-wave α-α resonant phase shift (i.e., the nuclear phase shift[39] with the hard sphere phase shift removed), and P is the S-wave penetrability factor. We find that the $L=0$ final state interaction contribution to the integrated yield in the energy region of the 2.9 MeV excitated state is approximately 60% of the ground state integrated yield. Although the accuracy of the Watson-Migdal theory is not well established, the results clearly indicate a major $L=0$ contribution to the 2.9 MeV state region, particularly when one considers that, at low re-

coil momenta, the $L=0$ yield is enhanced relative to $L=2$. In Fig. 8(e) we show the effect of adding in an $L=0$ contribution with about 33% of the ground state strength (the $L=2$ calculation has been normalized with a reasonable spectroscopic factor[38] of 0.72). Thus the difficulty with the 2+ state can clearly be qualitatively understood. Quantitative calculations similar to those of Ref. 22 go beyond the scope of the present paper. Clearly it would be of interest to have $(p,p\alpha)$ data leading to a 2+ state which is bound in order to see if the DWIA can reproduce the experimental data. The data at 156 MeV (Ref. 5) are not sufficiently precise to make a detailed investigation of the adequacy of the DWIA for $L=2$ transitions.

It should be noted that these same considerations should be applied to the ^{9}Be$(p,p\alpha)^5$He ground state transition, since this state is also unbound. However, the data presented represent a summation of the n-α relative energies of ~4 MeV (~3 MeV excitation in ^{5}He), and therefore contain essentially all of the $p_{3/2}$ resonance.[22] This summation in principle contains contributions due to other background phase shifts, such as $S_{1/2}$. In this case, as opposed to the ^{6}Li$(p,2p)^5$He reaction,[22] the $P_{3/2}$ resonance is excited by an $L=0$ transition which is greatly enhanced for small recoil momentum relative to the $L=1$ transition required for the excitation of the $S_{1/2}$ component. Thus contributions due to background phase shifts should be negligible, and the data in Fig. 8(c) represent the $\frac{3}{2}^-$ to $\frac{3}{2}^-$ transition.

We noted that in most cases at very large values of recoil momentum where the cross section is approximately one to two orders of magnitude smaller than the peak, the DWIA calculation tends to underpredict the cross section. This problem could be due to the use of improper optical potentials and/or the prescription used for the p-α cross section. Alternatively, there may be some effect due to the fact that in this region of large recoil momentum the p-α cross section is quite far off shell. This discrepancy may also represent some breakdown in the direct knockout treatment for cases where the direct DWIA cross section is small. However, since the cross sections in the region of the discrepancies are small compared to the peak value, we feel that agreement between theory and experiment is quite satisfactory.

C. Extraction of spectroscopic factors S_α

The normalization of the DWIA calculation to the experimental data provides the spectroscopic factor S_α. The values of S_α extracted from the data are presented in Table IV for each quasifree angle pair along with an estimate of the average

TABLE IV. Spectroscopic factors for quasifree angle pairs (θ_p/θ_α) extracted by means of the DWIA analysis. The errors reflect relative errors in both the three-body $(p,p\alpha)$ cross sections, and the two-body p-α on-shell cross section. The average S_α is a statistical average of all angles.

Reaction	θ_p/θ_α	S_α	$\langle S_\alpha\rangle^{\text{exp}}$	S_α^{theory}
^{6}Li$(p,p\alpha)^2$H	60/−52.7	0.66±0.04		
	75/−44.5	0.56±0.03		
	81.9/−40.9	0.59±0.04	0.58±0.02	1.0→1.0 [a]
	90/−36.8	0.49±0.04		
	105/−29.7	0.67±0.09		
^{7}Li$(p,p\alpha)^3$H	75/−45.3	0.92±0.07		
	81.3/−41.0	0.94±0.07	0.94±0.05	1.12 [b]
	105/−29.5	1.29±0.20		
^{9}Be$(p,p\alpha)^5$He	60/−52.4	0.46±0.04		
	75/−44.3	0.41±0.04		0.56 ($L=0$) [d]
	81.2/−41.0	0.43±0.04	0.45±0.02 [c]	0.55 ($L=2$) [d]
	90/−36.6	0.61±0.08		
	105/−30.9	0.83±0.15		
^{12}C$(p,p\alpha)^8$Be(0+)	75/−43.1	0.35±0.05		
	90/−35.7	0.59±0.09	0.59±0.05	0.56 [d]
	105/−28.7	0.81±0.14		

[a] Cluster model, Ref. 44.
[b] Reference 45.
[c] The spectroscopic factor used was the same for $L=0$ and $L=2$.
[d] Reference 38.

value of S_α. The error bars on each value of S_α are the result of the relative errors in the experimental $(p,p\alpha)$ data, as well as an estimate of the error in the two-body p-α cross section data in the particular angular range. Theoretical values of S_α are also listed in Table IV. We see that the agreement between experiment and theory in S_α is very good, in pronounced contrast to analyses utilizing PWIA calculations.

For ^{6}Li$(p,p\alpha)^2$H the spectroscopic factor of ~0.6 is somewhat lower than simple cluster model predictions, but in rather good agreement with recent work of Jain *et al.*[14] and Noble.[40] In addition, the normalization of the asymptotic tail of the ^{6}Li$\rightarrow\alpha+d$ wave function $\{S_\alpha^{1/2} R_{\alpha L}(r)\}$ agrees to within 13% with that obtained by Plattner, Bornand, and Alder[41] in a model-independent analysis of $\alpha+d$ elastic scattering. The spectroscopic factor for ^{7}Li$(p,p\alpha)^3$H on the other hand is very close to that predicted by simple LS coupling shell model predictions.

For ^{9}Be$(p,p\alpha)^5$He the extracted spectroscopic factor is in quite good agreement with the predictions of Kurath.[38] Also, in the case of ^{12}C$(p,p\alpha)^8$Be(0+) the extracted spectroscopic factor agrees very well with the predictions of Kurath.[38]

Thus, overall the agreement between theory and experiment is excellent, and further confirms the validity of DWIA analysis of $(p,p\alpha)$ reactions as a means of obtaining α-particle spectroscopic factors. It should be noted that, in contrast to most transfer reaction analyses, one can obtain absolute values for S_α.

D. Sensitivity of S_α to details of DWIA calculations

In addition to the difficulties observed in the factorization approximation which lead to uncertainties in the spectroscopic factor S_α, the S_α are sensitive to various uncertainties in the ingredients of the DWIA calculation. In particular they are sensitive to the parametrization of the bound α-particle potential and the optical model potentials for the entrance and exit channels. We have investigated the sensitivity of the DWIA cross sections to changes in these parameters in order to gain insight into the accuracy of the extracted spectroscopic factors.

In the DWIA the overlap between the initial and final nuclei has been represented by binding an α particle in a Woods-Saxon well. This procedure is common to both knockout and transfer reactions. Clearly an improved theoretical treatment is desirable. In the present work we have used the folding model to obtain the geometrical parameters (r_0, a) of the well. In order to investigate the sensitivity of the DWIA calculations, and therefore the S_α, to the bound state parameters, we have changed the radius parameter r_0 by ±0.2 fm about the central value listed in Table III. The primary effect on the DWIA cross section lies in the magnitude, the shape change being small compared to the experimental errors. In Fig. 9 we present the ratio of the DWIA cross sections $\sigma(r_0 \pm 0.2)/\sigma(r_0)$ for the four ground state transitions. The cross sections for the $L=0$ transitions correspond to $p_B = 0$ MeV/c, while for $L=1$ we chose the peak cross section ($p_B \simeq 60$ MeV/c). For ^{6}Li the variation in cross section is very small, for ^{7}Li and ^{9}Be it is ~±15%, and for ^{12}C it is ~±25%. Overall for these p-shell nuclei the sensitivity to the bound state radius is not particularly large, and does not introduce a significant uncertainty in the spectroscopic factor. For heavier targets the sensitivity to the bound state radius increases,[5] and a better understanding of the cluster wave function will be needed in order to extract good quantitative spectroscopic information.

In order to examine the sensitivity of the calculations to the optical potentials we have performed calculations with different sets of optical potentials. As in the case of the bound state, the primary effect is on the magnitude of the cross sections. The use of a different proton potential (from the same references) in the exit channel leads to a 3% reduction in the ^{9}Be cross section, and a 10% reduction in the ^{12}C cross section. The effect for ^{6}Li and ^{7}Li is comparable to that for

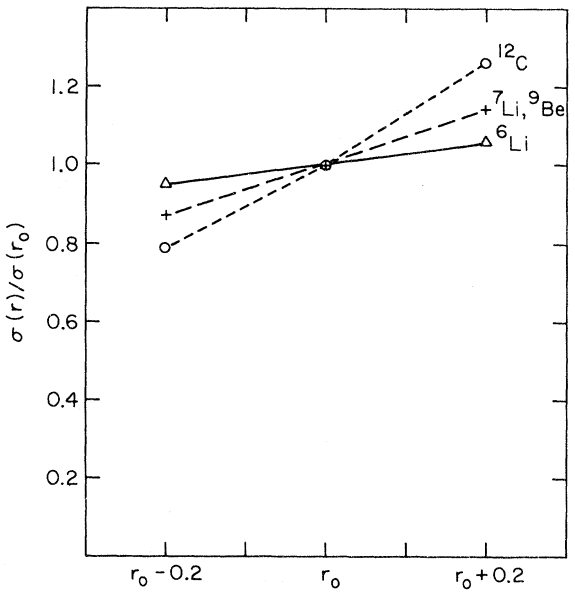

FIG. 9. Ratio of the DWIA cross section at zero recoil momentum for variations of ±0.2 fm in the radius parameter r_0 of the bound α-particle potential.

^{9}Be. Similar changes in the entrance proton channel produce similar effects. Thus changes in the optical potentials for the proton channels appear to lead to quite a small ($\leq 10\%$) change in the spectroscopic factor.

For the α channel, it is very difficult to find other suitable optical model potentials. For ^{9}Be and ^{12}C we have used an optical potential from Ref. 42 obtained from fitting $\alpha + {}^{12}$C elastic scattering data. The use of this potential leads to a ~15% increase in the ^{9}Be cross section and a ~6% increase in the ^{12}C cross section. In addition we have used an optical potential from Ref. 43 obtained from fitting ^{3}He + ^{6}Li data at 70 MeV, arguing that the ^{3}He potential may well be similar to the α potential. This potential leads to ~19% increase for ^{9}Be and ~25% increase for ^{12}C. Thus for ^{9}Be and ^{12}C we expect variations in optical potentials to lead to at most a 25% uncertainty in S_α. Due to the reduced distortion effects for ^{6}Li and ^{7}Li, we expect the uncertainty to be less for these target nuclei.

From these studies, we conclude that variations in the DWIA parameters are comparatively unimportant for these p-shell nuclei, although greater difficulties arise with increasing target mass (see, e.g., Ref. 5). Although there is a theoretical question of the appropriateness of the bound state treatment, we feel that uncertainties in the S_α from the present analysis are certainly less than a factor of 2, even for ^{12}C.

V. SUMMARY AND CONCLUSIONS

We have made a detailed experimental study of the three-body cross sections for the $(p,p\alpha)$ reaction on the p-shell nuclei ^{6}Li, ^{7}Li, ^{9}Be, and ^{12}C. These data provide a stringent test of the reaction mechanism. With the exception of a relatively small breakdown in the factorization approximation for ^{9}Be and ^{12}C, the data are in extremely good agreement with DWIA calculations. Absolute spectroscopic factors extracted by means of the DWIA analysis are in excellent agreement with theoretical predictions, indicating little evidence for clustering beyond that predicted by the shell model. In addition, careful studies of the sensitivity of the extracted spectroscopic factors to the details of the DWIA analysis were made. Considering uncertainties in the factorization and the various parameters in the DWIA calculations but excluding those involved in the treatment of the cluster wave function, we expect the spectroscopic factors to be accurate to better than a factor of 2.

These data and the present analysis provide strong support for the utilization of the $(p,p\alpha)$ reaction at bombarding energies near or above 100 MeV in order to obtain *absolute* spectroscopic information on α clustering in nuclei. The $(p,p\alpha)$ reaction studies coupled with a DWIA analysis can provide quantitative α-structure information in most cases more precise than that obtained from equivalent transfer reactions. In addition, the flexibility afforded by the three-body reaction presents the opportunity to make a much more detailed test of the reaction mechanism.

ACKNOWLEDGMENTS

We are indebted to the Cyclotron staff for their efforts during the experimental work, and to our colleagues at the University of Maryland for many stimulating discussions. Calculations were carried out using the UNIVAC 1108 of the Computer Science Center of the University of Maryland. We gratefully acknowledge their generous allocation of computer time.

---

*Work supported in part by the U.S.E.R.D.A.

†On leave of absence from the Council for Scientific and Industrial Research, Pretoria, South Africa.

‡ Present address: 190 Beaverdam Dr., Winterville, Georgia 30683.

[1]See e.g., M. Epstein *et al.*, Phys. Rev. 178, 1698 (1969); M. B. Epstein, J. R. Quinn, S. N. Bunker, J. W. Verba, and J. R. Richardson, Nucl. Phys. A169, 337 (1971); J. R. Quinn, M. B. Epstein, S. N. Bunker, J. W. Verba, and J. R. Richardson, *ibid.* A181, 440 (1972).

[2]M. Riou, Rev. Mod. Phys. 37, 375 (1965).

[3]B. Gottschalk and S. L. Kannenberg, Phys. Rev. C 2, 24 (1970); S. L. Kannenberg, Ph.D. thesis, Northeastern University (unpublished).

[4]D. Bachelier *et al.*, Phys. Rev. C 7, 165 (1973).

[5]D. Bachelier *et al.*, Nucl. Phys. A268, 488 (1976).

[6]M. Jain *et al.*, Nucl. Phys. A153, 49 (1970).

[7]J. W. Watson *et al.*, Nucl. Phys. A172, 513 (1971).

[8]D. F. Jackson and T. Berggren, Nucl. Phys. 62, 355 (1965).

[9]K. L. Lim and I. E. McCarthy, Nucl. Phys. 88, 433 (1966).

[10]R. K. Bhowmik, C. C. Chang, J. P. Didelez, and H. D. Holmgren, Phys. Rev. C 13, 2105 (1976).

[11]B. K. Jain and D. F. Jackson, Nucl. Phys. A99, 113 (1967).

[12]G. Jacob and T. A. J. Maris, Rev. Mod. Phys. 38, 121 (1966); 45, 6 (1973).

[13]A. K. Jain, N. Sarma, and M. Banerjee, Nucl. Phys. A142, 330 (1970).

[14]A. K. Jain *et al.*, Nucl. Phys. A216, 519 (1973).

[15]P. G. Roos *et al.*, Nucl. Phys. A257, 317 (1976).

[16]N. S. Chant and P. G. Roos, Phys. Rev. C 15, 57 (1977), preceding paper, referred to as I.

[17]N. S. Chant and P. G. Roos, in *Proceedings of the*

Second International Conference on Clustering Phenomena in Nuclei, College Park, 1975, edited by D. A. Goldberg, J. B. Marion, and S. J. Wallace (ERDA Technical Information Center, Oak Ridge, Tennessee), p. 265.

[18]P. G. Roos and N. S. Chant, in *Proceedings of the Second International Conference on Clustering Phenomena in Nuclei, College Park, 1975,* edited by D. A. Goldberg, J. B. Marion, and S. J. Wallace (ERDA Technical Information Center, Oak Ridge, Tennessee), p. 242.

[19]University of Maryland Cyclotron Laboratory Progress Report, 1972 (unpublished), p. 104.

[20]University of Maryland Cyclotron Laboratory Progress Report, 1971 (unpublished), p. 10.

[21]P. Frisbee and N. R. Yoder, University of Maryland Technical Report No. 73-043, 1973 (unpublished).

[22]Ranjan Bhowmik, C. C. Chang, H. D. Holmgren, and P. G. Roos, Nucl. Phys. A226, 365 (1974); C. C. Chang, R. Bhowmik, N. S. Chant, and P. G. Roos, Nucl. Phys. (to be published).

[23]L. G. Votta, P. G. Roos, N. S. Chant, and R. Woody, III, Phys. Rev. C 10, 520 (1974).

[24]H. G. Pugh *et al.*, Phys. Rev. Lett. 22, 408 (1969).

[25]A. Guichard *et al.*, Phys. Rev. C 4, 700 (1971).

[26]D. V. Meboniya, Phys. Lett. 30B, 153 (1969).

[27]A polynomial fit in angle and energy was made to the available $p+\alpha$ elastic scattering data from 49 to 156 MeV; B. W. Davies, M. K. Craddock, R. C. Hanna, Z. J. Moroz, and L. P. Robertson, Nucl. Phys. A97, 241 (1967); A. M. Cormack, J. N. Palmieri, N. F. Ramsey, and Richard Wilson, Phys. Rev. 115, 599 (1959); J. N. Palmieri, R. Goloskie, and A. M. Cormack, Phys. Lett. 6, 289 (1963); Ref. 23; W. Selove and J. M. Teem, Phys. Rev. 112, 1658 (1958); N. P. Goldstein, A. Held, and D. G. Stairs, Can. J. Phys. 48, 2629 (1970); R. Frascaria *et al.*, Phys. Rev. C 12, 251 (1975).

[28]A. M. Bernstein, Adv. Nucl. Phys. 3, 325 (1969), and references therein.

[29]P. Mailandt, J. S. Lilley, and G. W. Greenlees, Phys. Rev. C 8, 2189 (1973), and references therein.

[30]B. Buck, C. B. Dover, and J. P. Vary, Phys. Rev. C 11, 1803 (1975).

[31]T. Y. Li and S. K. Mark, Can. J. Phys. 46, 2645 (1968).

[32]G. S. Mani, D. Jacques, and A. D. B. Bix, Nucl. Phys. A165, 145 (1971).

[33]R. M. Devries, J.-L. Perrenoud, I. Šlaus, and J. W. Sunier, Nucl. Phys. A178, 424 (1972).

[34]P. Frisbee, Ph.D. thesis, University of Maryland, 1972 (unpublished).

[35]P. G. Roos, H. Kim, M. Jain, and H. D. Holmgren, Phys. Rev. Lett. 22, 241 (1969).

[36]In the final energy prescription each data set should be compared with p-α elastic scattering data at the final two-body energy; i.e., ^{6}Li (98 MeV), ^{9}Be (97 MeV), and ^{12}C (91 MeV). However, these differences are small.

[37]E. F. Redish, Phys. Rev. Lett. 31, 617 (1973).

[38]D. Kurath, Phys. Rev. C 7, 139 (1973).

[39]S. A. Afzal, A. A. Z. Ahmad, and S. Ali, Rev. Mod. Phys. 41, 247 (1969).

[40]J. V. Noble, Phys. Lett. 55B, 433 (1975).

[41]G. R. Plattner, M. Bornand, and K. Alder, Phys. Lett. 61B, 21 (1976).

[42]S. M. Smith *et al.*, Nucl. Phys. A207, 273 (1973).

[43]C. C. Chang (private communication).

[44]I. V. Kurdyumov, V. G. Neudatchin, and Yu. F. Smirnov, Phys. Lett. 31B, 426 (1970).

[45]Yu. F. Smirnov and D. Chlebowska, Nucl. Phys. 26, 306 (1961).